Filling an Emulsion Drop with Motile Bacteria

I. D. Vladescu,* E. J. Marsden,† J. Schwarz-Linek, V. A. Martinez, J. Arlt, A. N. Morozov, D. Marenduzzo, M. E. Cates, and W. C. K. Poon‡

SUPA and The School of Physics & Astronomy, The University of Edinburgh, King's Buildings, Mayfield Road, Edinburgh EH9 3JZ, United Kingdom

(Received 18 July 2014; revised manuscript received 21 October 2014; published 22 December 2014)

We have measured the spatial distribution of motile *Escherichia coli* inside spherical water droplets emulsified in oil. At low cell concentrations, the cell density peaks at the water-oil interface; at increasing concentration, the bulk of each droplet fills up uniformly while the surface peak remains. Simulations and theory show that the bulk density results from a "traffic" of cells leaving the surface layer, increasingly due to cell-cell scattering as the surface coverage rises above ~10%. Our findings show similarities with the physics of a rarefied gas in a spherical cavity with attractive walls.

DOI: 10.1103/PhysRevLett.113.268101 PACS numbers: 47.63.Gd, 82.70.Kj, 87.17.Jj, 87.18.Hf

The study of self-propelled particles [1], natural or synthetic "swimmers," is a part of the emerging field of "active matter physics" dealing with collections of intrinsically out of equilibrium entities. While problem-specific continuum theories exist [2], there is as yet no general recipe comparable to equilibrium free energy minimization for predicting the behavior of a general active matter system from knowledge of its microscopic constituents alone.

Confinement is of significant interest in diverse areas of physics. In active matter, it is already known that self-propelled particles can confine themselves spontaneously. Motile *Escherichia coli* and other bacteria encountering a surface continue to swim along it, giving rise to self-organised confinement to a 2D layer. Experimentally, the number density of motile *E. coli* between two parallel glass slides peaks strongly at the slides [3,4]. However, in this geometry, the cell density between the walls remains low and there is little 3D confinement, because the "wall-hugging" swimmers can escape essentially to infinity along the wall. Even the 2D confinement is weak: surface swimmers spread out to minimize interaction, and single-body physics suffices to explain wall hugging [3–6].

The interesting question now arises: what would happen if there is confinement in all spatial dimensions? Biologically, motile bacteria in nature are sometimes confined in this way, e.g., in raindrops [7] or infected host cells [8], possibly leading to motility loss [9]. In physics, the collective behavior of confined swimmers has attracted recent interest. At high density, motile *Bacillus subtilis* in a cylindrical drop develop stable vortices [10,11], while simulations of swimmers in a 2D box suggest novel forms of phase separation near close packing in the absence of hydrodynamic interactions [12]. In this work, we perform experiments starting from the opposite limit, and probe the way in which interaction effects emerge amongst motile bacteria confined within spherical emulsion droplets as their average density, ρ_0, increases from a small value.

As expected, at $\rho_0 \to 0$, we observe motile cells hugging the inner surface in a layer [3,4]. Instead, our focus here is on the unexpected way that the drop fills as ρ_0 increases: the bulk density increases uniformly while the surface peak remains. We present simulations and theory that reproduce essential features of our observations, and which suggest that the physics is reminiscent of a rarefied gas in a spherical cavity with attractive walls [13].

We studied spherical water-in-oil emulsion drops with a range of radii, R, containing a smooth-swimming mutant of *Escherichia coli* AB1157 bacteria in phosphate motility buffer at increasing average cell density, ρ_0. Green fluorescent protein expressed by the bacteria and a dye that preferentially adsorbs to the emulsifier on the water-drop surfaces allowed us to take high-resolution fluorescent confocal image stacks and reconstruct the cell positions inside droplets, Fig. 1 (cf. Supplemental Material movies

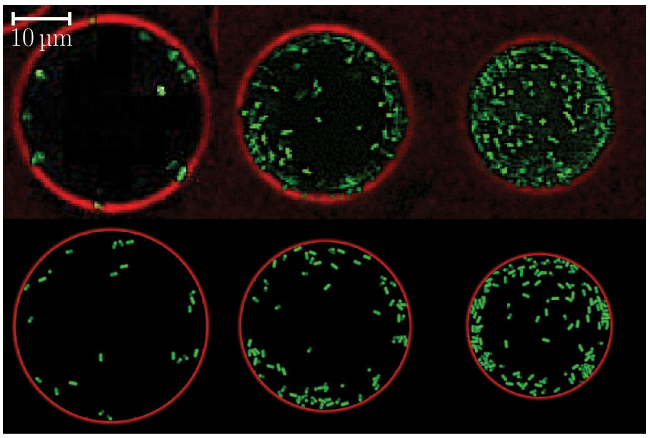

FIG. 1 (color online). Snapshots of 2 μm-thick cross sections of droplets, $(\phi, R) = 0.47\%$, 17.4 μm; 2.7%, 16.1 μm; 6.2%, 14.3 μm (left to right). Top: experiment, confocal images, ~2 μm below the equator, with red droplet edges and green bacteria. Bottom: simulated equatorial cross sections.

1 and 2 [14]). The majority of droplets had $R = 10$ μm 20 μm (Fig. S1), and are therefore significantly smaller than the persistence length of our swimmers (estimated to be $\lambda \gtrsim 100$ μm). *In situ* optical characterization using an oxygen-sensitive dye [25] and differential dynamic microscopy [26,27] confirmed the absence of oxygen gradients within these droplets and that cells swam during the duration of our experiments with essentially a constant speed distribution. Taking care to minimize aberration effects arising from working with spherical drops (Figs. S2, S3 [14]), we counted cells within concentric shells to obtain the cell density as a function of distance from the center, $\rho(r)$, which we assume to be isotropic. (See [14] for all preparative and imaging details.)

Typical density distributions, $\rho(r)$, for $R = (14 \pm 2)$ μm over a range of cell-body volume fraction, ϕ_0 [for (2×1) μm spherocylinderical cells] are shown in Fig. 2, with $\rho(r)$ normalized by the average number density ρ_0 and the radius by the droplet radius R. Each curve is the result of averaging over 10 stacks of analyzed images.

At low ϕ_0, bacteria are localized in a shell beneath the water-oil interface. Visually, almost all of these were motile, although a few nonmotile cells were also localized at this interface. As ϕ_0 increases, the peak in ρ/ρ_0 drops and migrates inward, while the cell density throughout the rest of the drop increases uniformly. This scenario occurs at all R studied (Fig. S4 [14]), although there was not enough statistics to investigate R dependence systematically. It is easily explained why our findings are independent of droplet size. We work with $2R < \lambda$; a qualitative change is only expected when droplets become larger than the swimmers' persistence length, λ.

While the $\rho(r)/\rho_0$ peak decreases with ϕ_0, Fig. 2, the absolute number of cells hugging the surface increases with ϕ_0. Figure 3 (inset) shows the total number of cells, N_s, found within the peak [28] plotted against the total number of cells, N_0. We report N_s as the total area the surface cells would cover as a monolayer, $N_s A_b$ (where $A_b =$ area covered by one cell), normalized by the droplet surface area ($A = 4\pi R^2$), $\eta = N_s A_b / A$ (the "surface area fraction"); N_0 is also reported as the total cell area NA_b similarly normalized, $\eta_0 = N_0 A_b / A$.

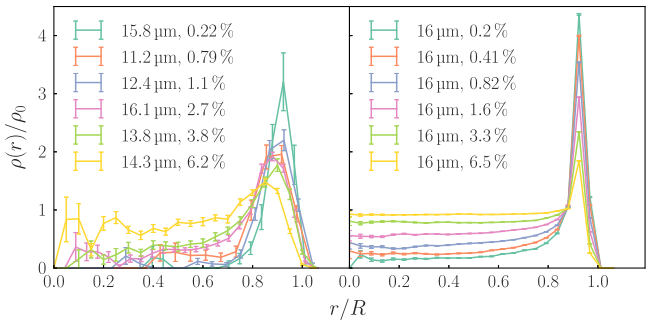

FIG. 2 (color online). Radial bacterial number density distributions, $\rho(r)$, normalized by the average number density of the whole droplet, ρ_0, plotted against the radial distance from the center, r, normalized by the droplet radius, R, averaged over 10 data sets. Left: Experimental data for $R \simeq 14$ μm. Right: Simulation data for $R = 16$ μm over a similar range of volume fractions as in experiment obtained for the case of maximal scattering at cell-cell collision.

Note that the peaks in Fig. 2 are much larger than crowding-induced layering in confined hard particles. For hard spheres in a rigid spherical cavity, there is no surface peak until $\phi_0 \gtrsim 20\%$ [29]; we see well-developed peaks at $\phi_0 \ll 5\%$ due to wall hugging [3,4] and not crowding.

The bulk of the droplet fills in a surprising way as ϕ_0 increases. Recent simulations [12] may suggest the interpretation that the wall layer is a high-density "liquid" phase coexisting with a low-density "vapor" phase in the bulk of the droplet. In this scenario, we should expect the interface between these two phases to move continuously inward as ϕ_0 is raised, as was observed for motile *B. subtilis* in a cylindrical droplet [10]. Instead, the bulk of our spherical droplets fill up uniformly with *E. coli* as ϕ_0 increases; see Fig. 2.

A qualitative explanation is as follows. At $\phi_0 \to 0$, cells are found almost exclusively at the inner droplet surface due to wall hugging [3–6]. This lower-density surface layer is as yet noninteracting. As ϕ_0 becomes finite and more and more cells arrive at the interface, the surface coverage eventually reaches a point when there will only be room for another cell if an existing surface cell leaves, spontaneously due to reorientation, or by scattering off the arriving cell or with another surface cell. Since $\lambda > 2R$ and the bulk density remains relatively low, a "departing" cell most likely travels along an approximately straight trajectory to

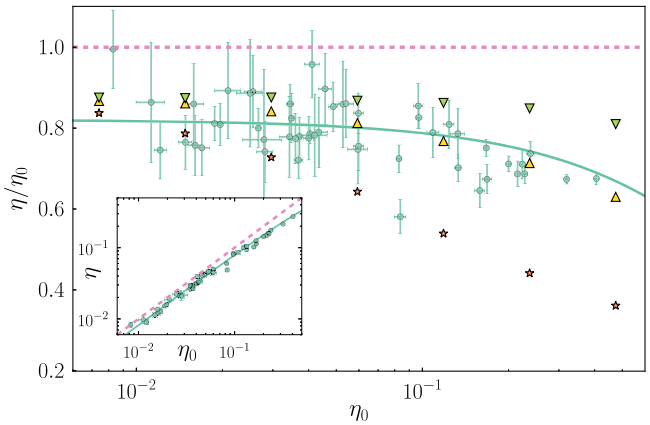

FIG. 3 (color online). The surface area fraction of bacteria, η, expressed as a fraction of the total potential surface coverage, η_0, as a function of η_0, from experiment (circle) and simulations ($\theta_r^{(c)} = 0$, downward triangle; $\theta_r^{(c)} \simeq 0.077$, upward triangle; $\theta_r^{(c)} = \pi$, star). Inset: The same data plotted in terms of the un-normalized surface coverage η: the absolute number of bacteria at the droplet surface increases sublinearly with the average cell density. Both plots: solid line denotes fit to Eq. (1); dashed line denotes total surface accumulation.

another part of the interface, where the process repeats. This cross-droplet traffic is manifested as a uniform increase in bulk density.

Consider first a simple analytical model for this picture. Bacteria with speed v give rise to a uniform flux towards a flat surface. We measure the bulk and surface concentrations using the equivalent area fractions η_0 and η already introduced, so that the inward flux is $\propto (\eta_0 - \eta)v$, where the factor $\eta_0 - \eta$ measures the number of cells in the bulk. We assume that an arriving cell will be trapped at the surface if it is presented with an empty surface, the latter with probability $\propto (1 - \eta)$. Thus, the arriving flux $\propto (1 - \eta)(\eta_0 - \eta)v$. Surface cells also swim with speed v, and remain trapped until they either leave spontaneously with probability $\propto \eta$ due to orientational fluctuations, or are scattered by other cells with probability $\propto \eta^2$. In the steady state, fluxes to and from the surface balance read as

$$(1 - \eta)(\eta_0 - \eta) = c\eta + b\eta^2; \qquad (1)$$

i.e., the arriving flux (left-hand side) is balanced (right-hand side) by cells leaving the surface due to spontaneous reorientation (c term) and scattering (b term). For swimmers of size $\sim a$ confined to a region of size $\sim R$, simple kinematics give [14] $c \simeq R/v\tau$, where τ is a typical reorientation time after which a surface cell spontaneously returns to the bulk, and $b \simeq kR/a$, where k is the probability that a surface cell-cell collision scatters a cell into the bulk.

To compare this simple kinetic model with experiments, we use Eq. (1) with $c = R/v\tau$ and $b = kR/a$ to fit the experimental data, Fig. 3 (•), taking into account that each point pertains to a droplet with a different R (Fig. S5 [14] shows the R dependence explicitly). This gives best-fit values $\tau_{\rm fit}^{-1} = (0.18 \pm 0.04)\ {\rm s}^{-1}$ and $k_{\rm fit} = 0.04 \pm 0.03$, the significant uncertainties in the latter quantity being a direct reflection of the rather noisy data. In our kinematic model, $\tau_{\rm fit}^{-1} = 0.18\ {\rm s}^{-1}$ is the rate at which trapped cells leave the surface due to spontaneous reorientation [14]; this is comparable to our estimate of the free rotational diffusion coefficient of a single flagellated cell, $D_r \simeq 0.2\ {\rm s}^{-1}$ [14]. The other parameter, $k_{\rm fit} = 0.04$, represents the probability of cell-cell scattering leading to a cell leaving the surface. This parameter is difficult to determine directly from observations, but visual inspection of Supplemental Material movies 1 and 2 [14] suggests that a k of a few percent is not unreasonable.

To compare directly with experimental data, we use the average droplet radius, $R = 16\ \mu$m, and average cell velocity, $v = 13.5\ \mu{\rm m\,s}^{-1}$ m, to find $c_{\rm fit} = 0.21$ and $b_{\rm fit} = 0.38$, and plot Eq. (1) as the full line in Fig. 3. The agreement is satisfactory, especially given the significant amount of noise in the data. In the Supplemental Material [14], we show that the predicted R dependence of the coefficients in Eq. (1) is also verified to within experimental uncertainties.

There are apparent similarities between our kinetic model, Eq. (1), and one proposed recently [30] to explain activity-driven phase separation [12]. However, the absence of particle-particle interaction in [12,30] gives rise to coexistence been liquid and vapor phases each of fixed density. On the other hand, the density dependence of the fluxes in Eq. (1) means that our surface layer and bulk densities change with the average cell concentration, and what we observed is incompatible with the coexistence of two phases with invariant densities.

We next simulated N_0 spherocylinders (end-to-end $\ell = 2\ \mu$m, diameter $0.8\ \mu$m) initially distributed uniformly inside a rigid sphere of radius R. Each cell self-propels at $v = 13.5\ \mu{\rm m\,s}^{-1}$ along its long axis and diffuses translationally and rotationally with isotropic diffusivities $D = 0.25\ \mu{\rm m}^2\,{\rm s}^{-1}$ and $D_r = 0.2\ {\rm s}^{-1}$ respectively, mimicking *E. coli*. Surface cells can reorient away from the surface with rotational diffusivity D_r.

What happens when two motile *E. coli* cells collide is likely very details dependent [6]. To access the essential physics, we simulated this process using a single phenomenological parameter, $\theta_{\rm r}^{(c)}$, the "angular deflection at collision": two colliding cells (bulk or surface) change their propulsion directions by an angle chosen uniformly from $[0, \theta_{\rm r}^{(c)}]$, and rotate around the original direction by an angle chosen uniformly in $[-\pi, \pi]$. The time step was 1 ms. (See [14] for details.)

If $\theta_{\rm r}^{(c)} = 0$, two colliding cells remain stuck until Brownian motion frees them. Since our data suggest that collision-induced movement of cells away from the surface layer is important, we explore first the opposite limit of maximal reorientation, viz., $\theta_{\rm r}^{(c)} = \pi$, which reproduces the most prominent aspects of the observed phenomenology (see Fig. 2): a peak in $\rho(r)/\rho_0$ that decreases as ϕ_0 increases, with a uniformly increasing bulk density.

The peak width, Δ, is narrower in simulations than in experiments. In the former, $\Delta \simeq 0.05R \simeq 1\ \mu$m, about half of the simulated cell length, $\ell = 2\ \mu$m. Previous simulations of wall hugging at moderate propulsion forces [5] have also found $\Delta \approx \ell/2$, which is explained as a remnant of the depletion zone next to a wall in the case of passive hard rods. The wider experimental peaks, $\Delta \simeq 3\ \mu$m, presumably result partly because real *E. coli* with flagella behave as rods considerably longer than $\ell = 2\ \mu$m. However, already-noted [14] near-edge optical aberrations may also contribute to the apparent Δ.

We turn next to the number of cells in the surface layer. As expected, the case of no collision-induced reorientation, $\theta_{\rm r}^{(c)} = 0$, gives a constant η/η_0 as η_0 increases, Fig. 3 (▼). This does not reproduce our data. Complete randomization at collision, $\theta_{\rm r}^{(c)} = \pi$, Fig. 3 (⋆), is more realistic. The actual data (•), which lie between these two limits, are accounted for by $\theta_{\rm r}^{(c)} \simeq 0.077$, Fig. 3 (▲). To make sense of this value,

note that the average reorientation at a cell-cell collision given by a particular value of $\theta_r^{(c)}$ can be recast as an effective collisional rotational diffusivity, $D_r^{(c)} = \theta_r^{(c)}/6\Delta t$, where $\Delta t = 1$ ms is our time step [14]. Thus, our data suggest $D_r^{(c)} \simeq 1\ \mathrm{s}^{-1}$, which is about five times the Brownian D_r. The plots of $\rho(r)/\rho_0$ at various cell densities at this value of $\theta_r^{(c)}$ (Fig. S6 [14]) display the same phenomenology as those shown in Fig. 2, although the uniform rise of the bulk density with ϕ_0 is not as rapid as observed.

It would be unrealistic to expect our simple simulated model to reproduce exactly the totality of the data shown in Figs. 2 and 3. Most importantly, the details of surface swimming depends sensitively on precise geometric parameters of the swimmers [31]. Furthermore, the distance between a wall-hugging cell and the surface can fluctuate by up to a cell width or more [32,33], partly due to the complicated wobble of the cell body, and the effect of surface curvature remains largely unexplored. A basic model in which cells arriving at a surface simply align perfectly with it cannot be expected to account for such complexities, and therefore of the shape of the surface peak, Fig. 2. Such complexities may have less effect on an "integral measure" such as the total number of trapped cells, Fig. 3, which is indeed what we have fitted to theory and simulations.

Our system shows certain similarities with a confined classical rarified gas in which the mean free path, λ, is larger than or comparable to the confinement length, L, i.e., the Knudsen number, $\mathrm{Kn} = \lambda/L > 1$. In both cases the particles can traverse the confined space in a straight line. For hard spheres of radius a at volume fraction ϕ_0 confined to a sphere of radius R, $\mathrm{Kn} = 1/(6\sqrt{2}\phi_0 R/a)$ [13], which for the droplets reported in Fig. 2 ranges from $\mathrm{Kn} \simeq 1.9$ at $\phi_0 = 0.22\%$ through $\mathrm{Kn} \simeq 0.5$ at $\phi_0 = 0.79\%$ to $\mathrm{Kn} \simeq 0.06$ at $\phi_0 = 6.2\%$. Simulations [13] show that in a confined rarefied gas at $\mathrm{Kn} > 1$ with attractive walls, the evolution of the density profile as a function of average gas density is closely similar to that shown in Fig. 2: a broadening surface peak and uniformly increasing bulk density. The attraction in our case comes from wall hugging [3,4].

This analogy is no longer appropriate either at large ϕ_0 or when the persistence length of the swimmers drops below the system size, $\lambda/2R < 1$. The latter can be probed using wild-type cells, which tumble every 1 s or so between straight runs. Given $v \lesssim 20\ \mu\mathrm{m\,s}^{-1}$, we now have $\lambda \lesssim 20\ \mu$m. Figure 4 compares the density profile for a smooth swimmer in a drop with $2R \ll \lambda$, and a wild type in a drop with $2R > \lambda$. The density peak at the droplet edge has disappeared in the latter case, presumably because surface tumbles now remove cells from the trapped layer too rapidly for a peak to build up.

At cell densities 5–10 times higher than the maximum reported so far, we observed vortices with constantly changing orientations (Supplemental Material movie 3 [14]). This may be compared to *B. subtilis* confined to cylindrical water drops at high densities, where a single vortex aligned to the cylinder axis is seen [10]. The difference may partly be due to the greater length of *B. subtilis* cells, and partly to differing spatial symmetry. Such collective motion is left to future work.

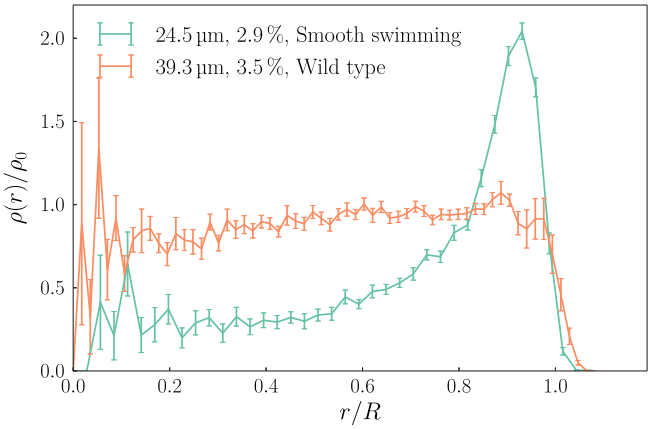

FIG. 4 (color online). Comparison of density profiles for smooth swimmers (red) and wild-type run-and-tumble cells (blue).

Finally, if internal flows from bacterial motility can set up exterior flows, then our droplets should display at least enhanced positional fluctuations. Tracking revealed no such activity. This is likely because the lecithin layer stabilizing each droplet is rigid enough to decouple internal and external flows.

To summarize, we have observed the emergence of many-body behavior in spherical water droplets filled with increasing density of motile *E. coli* bacteria. The single-body physics of previously studied wall hugging [3,4] together with Brownian reorientation taking cells from the surface into the bulk suffice to explain observations up to a surface coverage of $\eta_0 \simeq 0.1$, Fig. 3. Thereafter, the decrease of η/η_0 with η_0 evidences cell-cell scattering; fitting to a simple theory suggests that a few percent of collisions scatter cells from the surface layer to the bulk. Bulk traffic of cells from one part of the inner surface to another, initially due solely to Brownian reorientation, and then increasingly due to cell-cell scattering, explains the observed uniform increase in the bulk density as the average cell density increases.

We thank A. Brown, A. Dawson, D. Dell'Arciprete, A. Jepson, and T. Pilizota for discussions. The work was funded by the Royal Society, the UK Engineering and Physical Sciences Research Council (EP/I004262/1, EP/J007404/1), the European Union [FP7-PEOPLE (PIIF-GA-2010-276190)], and the European Research Council (ADG-PHYAPS).

*i.vladescu@ed.ac.uk
†e.j.marsden@ed.ac.uk
‡w.poon@ed.ac.uk

[1] W. C. K. Poon, in *Physics of Complex Colloids*, edited by C. Bechinger, F. Sciortino, and P. Ziherl (Società Italiana di Fisica, Bologna, 2013) pp. 317–386.
[2] M. C. Marchetti, J. F. Joanny, S. Ramaswamy, T. B. Liverpool, J. Prost, M. Rao, and R. Aditi Simha, Rev. Mod. Phys. **85**, 1143 (2013).
[3] G. Li and J. X. Tang, Phys. Rev. Lett. **103**, 078101 (2009).
[4] A. P. Berke, L. Turner, H. C. Berg, and E. Lauga, Phys. Rev. Lett. **101**, 038102 (2008).
[5] J. Elgeti and G. Gompper, Eur. Phys. Lett. **85**, 38002 (2009).
[6] K. Drescher, J. Dunkel, L. H. Cisneros, S. Ganguly, and R. E. Goldstein, Proc. Natl. Acad. Sci. USA **108**, 10940 (2011).
[7] T.-C. Yang, Y.-W. Leu, H.-C. Chang-Chien, and R.-M. Hu, J. Bacteriol. **191**, 2266 (2009).
[8] F. S. Southwick and D. L. Purich, BioEssays **16**, 885 (1994).
[9] K. M. Jones, H. Kobayashi, B. W. Davies, M. E. Taga, and G. C. Walker, Nat. Rev. Microbiol. **5**, 619 (2007).
[10] H. Wioland, F. G. Woodhouse, J. Dunkel, J. O. Kessler, and R. E. Goldstein, Phys. Rev. Lett. **110**, 268102 (2013).
[11] E. Lushi, H. Wioland, and R. E. Goldstein, Proc. Natl. Acad. Sci. USA **111**, 9733 (2014).
[12] X. Yang, M. L. Manning, and M. C. Marchetti, arXiv: 1403.0697.
[13] M. Cieplak, J. Koplik, and J. R. Banavar, Physica A (Amsterdam) **274**, 281 (1999).
[14] See Supplemental Material at http://link.aps.org/supplemental/10.1103/PhysRevLett.113.268101 for movies and details of the experiments and calculations, which includes Refs. [15–24].
[15] J. H. Miller, *Experiments in Molecular Genetics*, Bacterial genetics—E. coli (Cold Spring Harbor, New York, 1972).
[16] T. Baba, T. Ara, M. Hasegawa, Y. Takai, Y. Okumura, M. Baba, K. A. Datsenko, M. Tomita, B. L. Wanner, and H. Mori, Mol. Syst. Biol. **2** (2006).
[17] J. Sambrook and D. W. Russell, *Molecular Cloning: A Laboratory Manual* (Cold Spring Harbor, New York, 2001).
[18] M. A. Grompone, in *Bailey's Industrial Oil and Fat Products*, 6th ed. (Wiley, New York, 2004), pp. 655–730.
[19] R. Battino, in *Solubility Data Series* (Pergamom, New York, 1981).
[20] J. Schindelin, Nat. Methods **9**, 676 (2012).
[21] M. Doube, M. M. Kłosowski, I. Arganda-Carreras, F. P. Cordelières, R. P. Dougherty, J. S. Jackson, B. Schmid, J. R. Hutchinson, and S. J. Shefelbine, Bone (N.Y.) **47**, 1076 (2010).
[22] M. Schwertner, M. J. Booth, and T. Wilson, J. Microsc. **228**, 97 (2007).
[23] M. Laikin, *Lens Design*, Optical Science and Engineering, 4th ed. (CRC Press, Florida, USA, 2010).
[24] H. C. Berg, *Random Walks in Biology* (Princeton University Press, Princeton, NJ, 1993).
[25] H. C. Gerritsen, R. Sanders, A. Draaijer, C. Ince, and Y. K. Levine, J. Fluoresc. **7**, 11 (1997).
[26] L. G. Wilson, V. A. Martinez, J. Schwarz-Linek, J. Tailleur, G. Bryant, P. N. Pusey, and W. C. K. Poon, Phys. Rev. Lett. **106**, 018101 (2011).
[27] V. A. Martinez, R. Besseling, O. A. Croze, J. Tailleur, M. Reufer, J. Schwarz-Linek, L. G. Wilson, M. A. Bees, and W. C. K. Poon, Biophys. J. **103**, 1637 (2012).
[28] Throughout, the peak is taken to span $R_p < r < R$, where R_p is where the density first rises to $\rho = \rho_0$ coming from the center. Other reasonable algorithmic or visual definitions of "the peak" do not change our conclusions.
[29] S. T. Chui, Phys. Rev. B **43**, 11523 (1991).
[30] G. S. Redner, M. F. Hagan, and A. Baskaran, Phys. Rev. Lett. **110**, 055701 (2013).
[31] H. Shum, E. A. Gaffney, and D. J. Smith, Proc. R. Soc. A **466**, 1725 (2010).
[32] P. D. Frymier, R. M. Ford, H. C. Berg, and P. T. Cummings, Proc. Natl. Acad. Sci. USA **92**, 6195 (1995).
[33] G. Li, L. K. Tam, and J. X. Tang, Proc. Natl. Acad. Sci. USA **105**, 18355 (2008).